Cement & Concrete Composites 34 (2012) 147–155

Contents lists available at SciVerse ScienceDirect

Cement & Concrete Composites

journal homepage: www.elsevier.com/locate/cemconcomp

# Non-contacting strain measurement for cement-based composites in dynamic tensile testing

Deju Zhu [1], Barzin Mobasher *, S.D. Rajan

*School of Sustainable Engineering & the Built Environment, Arizona State University, Tempe, AZ 85287, United States*

ARTICLE INFO

*Article history:*
Received 17 May 2010
Received in revised form 11 September 2011
Accepted 12 September 2011
Available online 18 September 2011

*Keywords:*
Dynamic tensile testing
Laser extensometer
Phase-shift
Zero-crossing
Cement-based composites

ABSTRACT

This paper presents the development of a test procedure and application of non-contacting strain measurement for cement-based composites under moderately high strain rate tensile tests. The strain time histories of test specimens measured by a laser extensometer in high speed mode were derived by a phase-shift technique based on zero-crossing method. The accuracy of the linear variable differential transformer (LVDT) of the actuator in a servo-hydraulic high rate testing machine was verified by image analysis using sisal fiber reinforced cement composite at a strain rate of 25 $s^{-1}$. The same procedure was then applied to Alkaline Resistant (AR) glass fabric reinforced cement composite tested at an average strain rate of 17 $s^{-1}$. Comparison between the strain values measured by the laser extensometer and the LVDT shows a good agreement between these two measurement techniques. The test results show that the Young's modulus, tensile strength, maximum strain, and toughness of the AR-glass fabric–cement composite increase with increasing strain rate. However, under both static and dynamic loadings the composite has similar behavior: multi-crack development and one dominant crack leading to final failure. In order to ensure the accuracy of dynamic tensile test procedures, non-contacting devices and techniques should be used as an independent means of verification of test results. The accuracy required in quantifying relative improvements in mechanical properties necessitates the various methods of measuring the displacement and strain rate properties.



## 1. Introduction

Understanding the mechanical properties of engineering materials at varying strain rates is necessary for proper design of products for structural, military, construction, and sports applications. Materials loaded at high strain rates exhibit mechanical characteristics that are different from those obtained under quasi-static loading. The strain rate dependency of various materials has been known since the 19th century and mechanical responses under high strain rate, blast, or shock have undergone careful investigations. A number of experimental techniques exist for high strain rate material properties that include split Hopkinson bar devices [1,2], falling weight devices [3], flywheel facilities, and servo-hydraulic machines [4,5]. Measurement of deformation plays an important role in establishing the dynamic behavior of materials and as such, direct measurement of strain is challenging at high strain rates. Traditional strain measuring techniques rely on the use of extensometers and strain gages [6,7] which must be verified for each specific specimen configuration, test temperature, loading rate, and strain range. Non-contacting strain measuring techniques are preferred in many situations and include laser extensometer [8], digital laser speckle technique [9], rotating drum of high speed camera [10], diffraction-grating technique [11] and image correlation technique [12,13].

Cementitious construction products may be subjected to dynamic loading resulting from blast explosions, projectiles, earthquakes, and machine vibrations. In order to accurately analyze and design these structures, it is necessary to properly characterize the load and displacement responses measured in consideration to the applied strain rates, especially when energy absorption properties are of concern. The inherent brittleness and low tensile strength of most cement-based elements results in severe distributed damage and cracking under dynamic loading. Fiber reinforcement is clearly an effective way to enhance the tensile resistance, strength, and energy absorption under dynamic loading [14,15]. Textile reinforced cement composites have demonstrated significant energy absorption capacity under static and dynamic loading as compared to plain and fiber cement composites [16,17] but their dynamic tensile behavior is still not well documented. This is partly because different researchers have used different characterization techniques for strain measurements and toughness calculations.

* Corresponding author. Tel.: +1 480 965 0141; fax: +1 480 965 0557.
*E-mail addresses:* Deju.Zhu@asu.edu (D. Zhu), Barzin@asu.edu (B. Mobasher), S.Rajan@asu.edu (S.D. Rajan).
[1] Present address: McGill University, Montreal, QC, Canada.

0958-9465/$ - see front matter © 2011 Elsevier Ltd. All rights reserved.
doi:10.1016/j.cemconcomp.2011.09.011

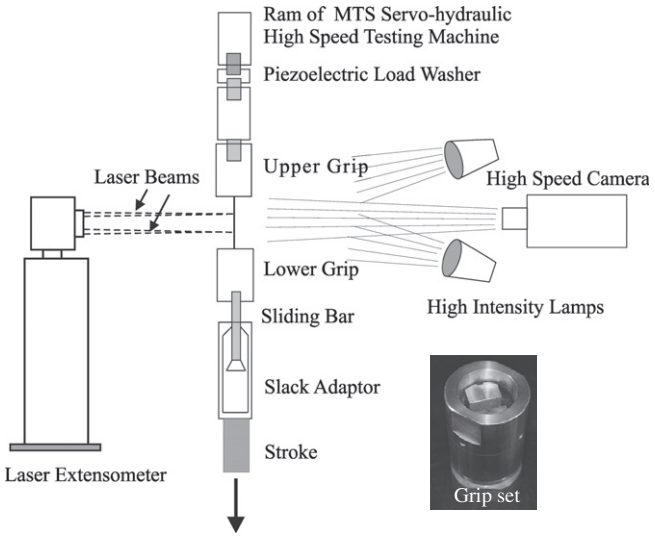


**Fig. 1.** Schematic diagram of the setup for dynamic tensile test.

Most of the available literature on the dynamic tensile behavior of concrete are based on plain concrete in compression and limited data supporting increase in tensile strength [18,19]. Dynamic tensile data on fiber and fabric reinforced concrete are even more limited. Kim et al. [20] investigated the strain rate effect on the tensile behavior of high performance fiber reinforced cement composites (HPFRCC) using two deformed high strength steel fibers, namely hooked fibers and twisted fibers at pseudo static (strain rate of $1 \times 10^{-4}\,s^{-1}$) and seismic (strain rate of $0.1\,s^{-1}$) loading conditions. The tensile behavior of HPFRCC with twisted fibers was sensitive to the strain rate, while hooked fiber reinforced specimens showed no rate sensitivity. Silva et al. [21] performed high speed tensile tests in sisal fiber reinforced cement composites at a strain rate of $24.6\,s^{-1}$. Pronounced strain-rate dependence was noted for toughness and failure strain due to the pullout fracture behavior of the material. Zhu et al. [22] investigated three types of fabric reinforced cement composites at the strain rates of $10–25\,s^{-1}$ using a servo-hydraulic high rate testing machine. Composites reinforced with carbon fabric exhibited the highest modulus, strength, failure strain and toughness compared to glass and polyethylene fabric reinforced composites. Mechtcherine et al. [23] studied the dynamic behavior of strain-hardening cement-based composites (SHCC) reinforced with Polyvinyl Acetate (PVA) fibers under tensile load. For tensile tests performed at strain rates up to $1 \times 10^{-2}\,s^{-1}$, SHCC exhibited an increase in tensile strength and a decrease in strain capacity with increasing strain rate. When loaded at high strain rates ranging from 10 to $50\,s^{-1}$, SHCC showed an increase in both tensile strength and strain capacity with increasing loading rate. More recently, Silva et al. [24] presented results of textile-reinforced concrete (TRC) with and without short glass fibers in the matrix subjected to both low and high-rate tensile loading ranging from $1 \times 10^{-4}$ to $50\,s^{-1}$. An increase in tensile strength, strain capacity, and work-to-fracture was observed with increasing strain rates up to $0.1\,s^{-1}$. For strain rates above $5\,s^{-1}$, an increase in the tensile strength and work-to-fracture was also observed, but there was a decrease in the strain capacity.

Depending on the methodology used in measurement of sample displacement, the values of strain rates may significantly depend on the test set up. Several dynamic tensile test results have used the linear variable differential transformer (LVDT) of the actuator in the servo-hydraulic high rate testing machine [21–24]. The

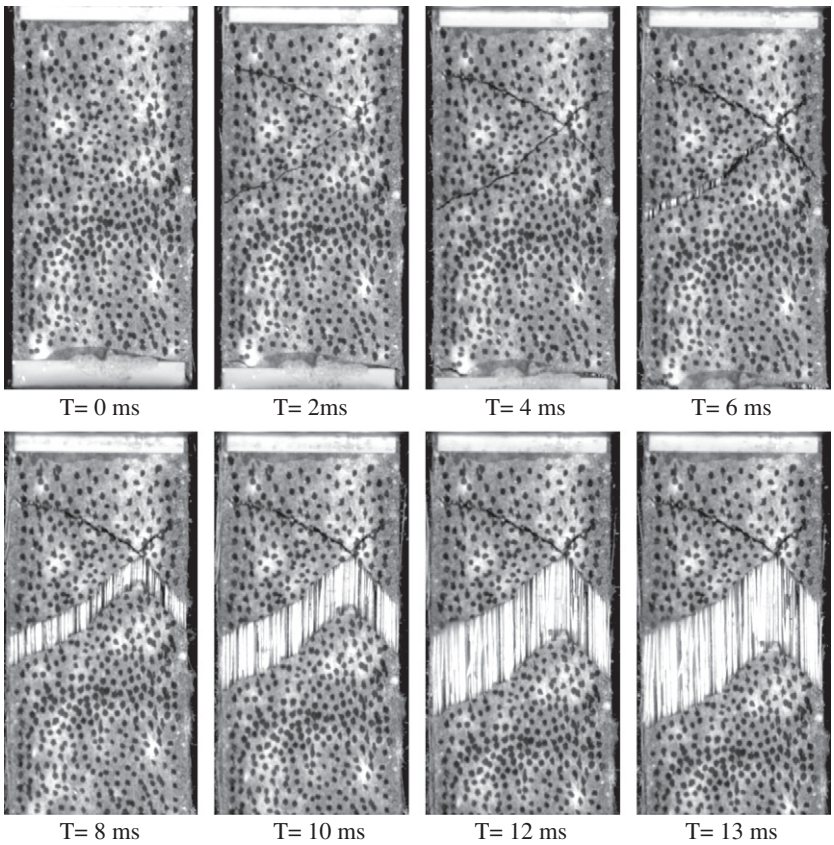


**Fig. 2.** Speckle pattern and failure behavior of sisal fiber cement composite under dynamic loading.

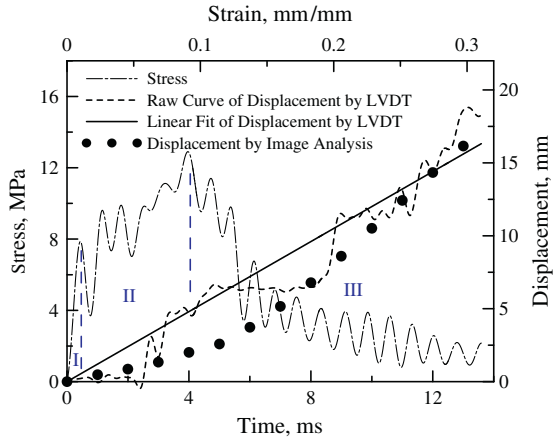


**Fig. 3.** Stress–strain and displacement–time curves of sisal fiber cement composite obtained by Stroke LVDT and image analysis (DIC).

accuracy of the measurement is affected by the compliance and inertial effects of the testing fixtures and may differ from testing machine to machine. At high strain rates, Borsutzki et al. [25] recommended strain measurement at high strain rates to be done by the relative displacement measured from points other than the gauge section of the specimen, i.e. the displacement between grips or the actuator displacement measured by LVDT. In order to ensure the dynamic tensile testing accuracy, non-contacting devices and techniques should be used as an independent means of verification of test results.

The present work presents a data processing procedure using a laser extensometer and its application to cement-based composites tested at moderately high strain rates. The paper is organized as follows. The challenges in the use and application of LVDT measurement and image analysis techniques in dynamic tensile testing are discussed first. The basic principles of laser measurement and phase-shift method are described next. Failure behavior of alkali resistant (AR)-glass fabric-composite at an average strain rate of 17 $s^{-1}$ is used as an example to illustrate how the developed technique can be used for similar textile reinforced composites. Strain rate effects are compared with the responses obtained from static loading cases.

## 2. Dynamic tensile testing

### 2.1. Dynamic test setup

Dynamic tensile tests are conducted on a servo-hydraulic high rate testing machine in open-loop control with a maximum loading speed of 14 m/s. Fig. 1 shows the schematic diagram of the setup for dynamic tensile test. The load is measured by a piezoelectric load washer (Kistler 9041A) with a capacity of 90 kN. A sudden displacement is introduced at the lower grip through a slack adaptor. The displacement is measured by a high accuracy Trans-Tek LVDT attached to the actuator and is referred to as Stroke LVDT. The Stroke LVDT is excited by a high speed signal conditioning amplifier with a frequency of 10 kHz to insure the accuracy of position measurement [26]. A high speed digitizer is used to collect the signals from the load washer, the Stroke LVDT and the laser extensometer at a sampling rate of 10 MHz. This high rate allowed the digitizer to collect transient 250 kHz signals from the laser extensometer without signal aliasing [27]. The Stroke LVDT signal contains high frequency noise and is filtered by a finite impulse response (FIR) digital low-pass filter with a cutoff frequency of

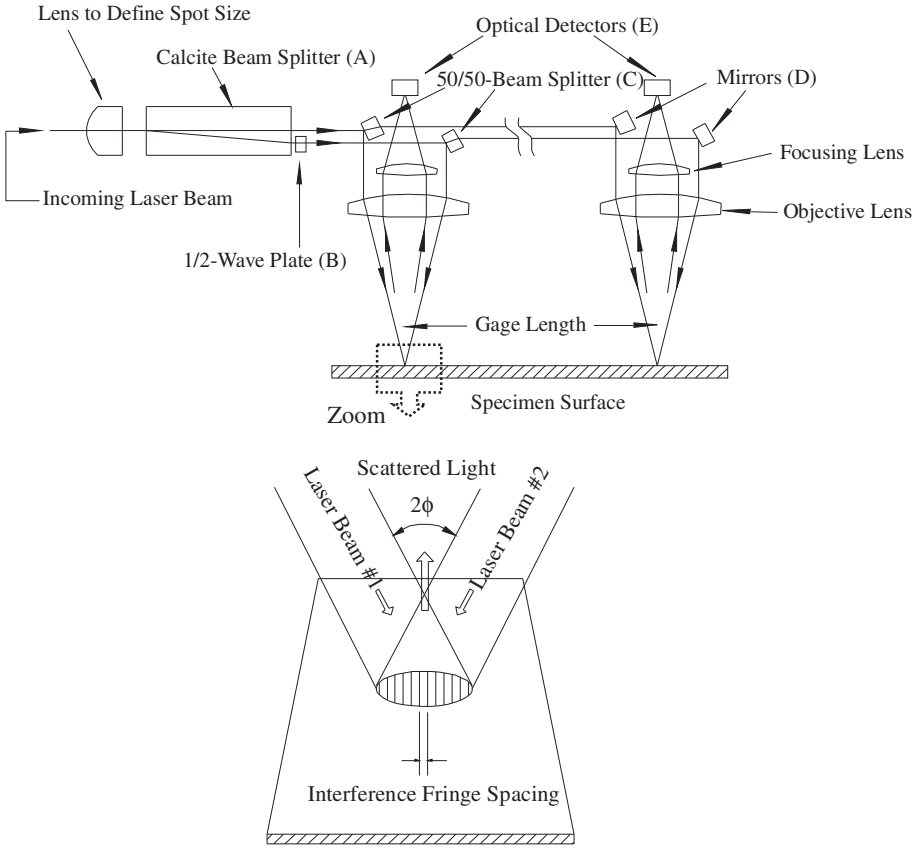


**Fig. 4.** Optical layout of laser extensometer and interference fringe.

3 kHz to eliminate the noise. Details of signal conditioning have been addressed in an earlier work [28]. A high speed digital camera (Phantom v.7) is also used to record sample deformation and failure during tests. This allows a direct comparison of the Stroke LVDT measurement with the laser extensometer data and image analysis.

### 2.2. Strain measurement using digital image correlation (DIC) method

As a full-field approach, image analysis techniques are widely used in displacement and strain field measurement and are a powerful tool to post-process fringe images generated by Moiré effect, photo-elastic materials or interferometric methods [29]. Digital image correlation (DIC) was proposed by Peters and Ranson [30] in early 1980s. By performing digital image processing on the images of the test specimen before and after applying loads, the entire displacement field can be constructed. Image correlation technique is a fundamental concept of computer vision recognition based on light intensity pattern matching within a small area in the undeformed image and the same area in the deformed image [31,32]. An approach based on digital image correlation (DIC) was applied to cement composites by Mobasher and Rajan [33]. This procedure was used to verify the accuracy of the displacement measurements. The light intensity patterns that are based on 256 gray levels, are converted to continuous intensity patterns using a bi-linear interpolation approach. A high speed digital camera (Phantom v.7) was used to record sample deformation at a sampling rate of 10,000 fps for tests conducted at a moderately high strain rate (strain rate = 25 $s^{-1}$).

### 2.3. Nature of deformation in cement composites under dynamic tensile loading

Earlier publications on cement composites under dynamic loading [21–24] revealed various operative modes and mechanisms during the test. These mechanisms include uniform deformation, distributed cracking, shear cracking, fiber pullout, and localization of deformation. Experiments show that due to the changes in the rate of displacement both in terms of spatial and temporal terms, definition of a single strain rate parameter may not be appropriate.

Some of these stages of cracking in a continuous fiber cement system under dynamic load are shown in Fig. 2. The details of test setup and the composite materials used for image analysis were discussed by Silva et al. [21]. Speckle pattern was generated on the surface of cement composites to create a uniform contrast (Fig. 2). Fig. 3 shows the stress–strain curve and the failure behavior of sisal fiber cement composite under dynamic loading (strain rate = 25 $s^{-1}$). Both tensile and shear cracks are observed at different stages in the sample, and the composite failure is a result of crack widening leading to fiber pullout. Tensile and shear cracks were also observed under static loading (see Ref. [21]). As the cracking saturates, progressive interfacial damage develops due to crack widening and ultimately leading to failure by fiber pullout.

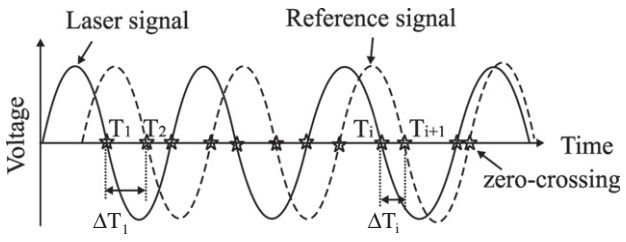


**Fig. 5.** Phase shift between reference signal and second signal.

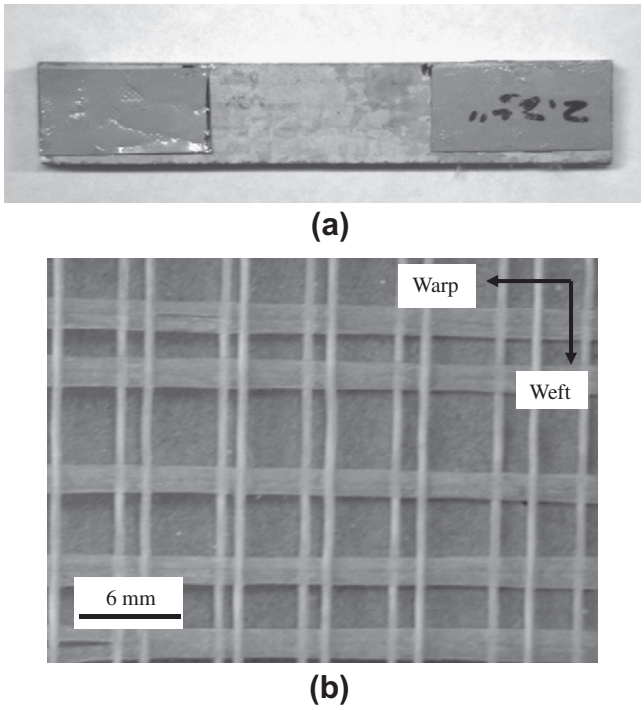


**Fig. 6.** (a) AR-glass fabric reinforced cement composite, and (b) AR-glass fabric.

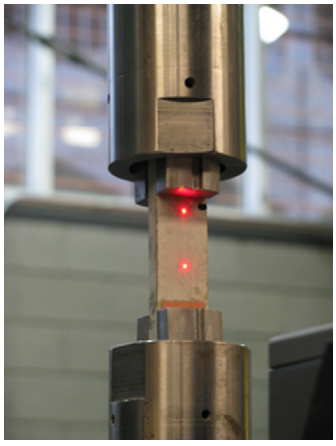


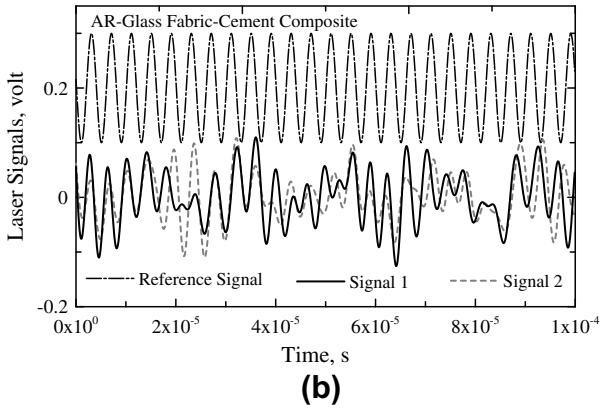


**Fig. 7.** (a) Test setup using AR-glass fabric-cement composite, and (b) a small portion of sinusoidal signals generated by laser extensometer and high speed accessory after receiving scattered light from the composite.

Note that proper definition of singular strain rates may not be applicable in this case. In order to further evaluate the response one has to use alternative methods of displacement measurement and differentiate the various local and average properties.

In addition to stress vs. time curve, Fig. 3 also compares the displacement–time curves by the Stroke LVDT and image analysis. The dynamic tensile response can be divided into three regions: (i) elastic region; (ii) strain hardening region; and (iii) strain softening region. Region I shows the linear elastic response characterized by an average modulus of 1 GPa. Region II is marked by the strain hardening behavior with the formation of cracks, and by the stress oscillations due to system ringing [26]. In the strain softening region (strain $\varepsilon = 0.10$–$0.32$ mm/mm), the stress decreases due to the failure of both matrix and the fibers. At this stage, the fiber debonding and pullout from the matrix leads to widening of certain cracks. The definition of a constant strain rate is not applicable since the displacement along the length of the sample is no longer uniform. At the end ($t = 13$ ms, $\varepsilon = 0.3$ mm/mm) a residual strength of 2 MPa due to the frictional fiber–matrix bond strength is observed resulting in an enormous energy absorption capacity in the strain softening region. The energy absorption capacity is as much as seven times higher than the static tests [21].

The displacement value obtained by image analysis at a certain time step, indicated by a solid circle in Fig. 3, is the maximum displacement along the specimen. The displacement obtained by image analysis is nonlinear as a function of time and less than that of linear fit of displacement obtained by the Stroke LVDT during the majority of the test duration. Note that although the deformation imposed is unidirectional, due to axial oscillations of the high speed machine, the oscillations remain an integral part of the test method. As the specimen starts to fail in region III, the difference in the displacement obtained by image analysis and the Stroke LVDT reduces significantly and became negligible after 11 ms ($\varepsilon = 0.25$ mm/mm). Therefore, the maximum displacement (and similarly for maximum strain) obtained by the Stroke LVDT represents the real response of the test specimen when it totally fails. This comparison however is not quite valid during the early stages of the testing phase. In the following discussion, the strain values obtained by the Stroke LVDT are used to construct the stress–strain curves of AR-glass fabric–cement composite.

## 3. Development and verification of non-contacting strain measurement

### 3.1. Basic principles of laser measurement

In order to increase the frequency response of the measurement system, a laser extensometer manufactured by Optra Inc. (Model 3000) was used. Fig. 4 shows the optical layout of measurement method. The incoming laser beam is comprised of two collinear, orthogonally polarized components which differ in frequency by exactly 250 kHz. After passing through a calcite beam splitter (A), the laser beam divides into two, with one directed through a half wave plate (B) which rotates the polarization vector by 90°, thus allowing it to interfere with the unaltered beam to create an

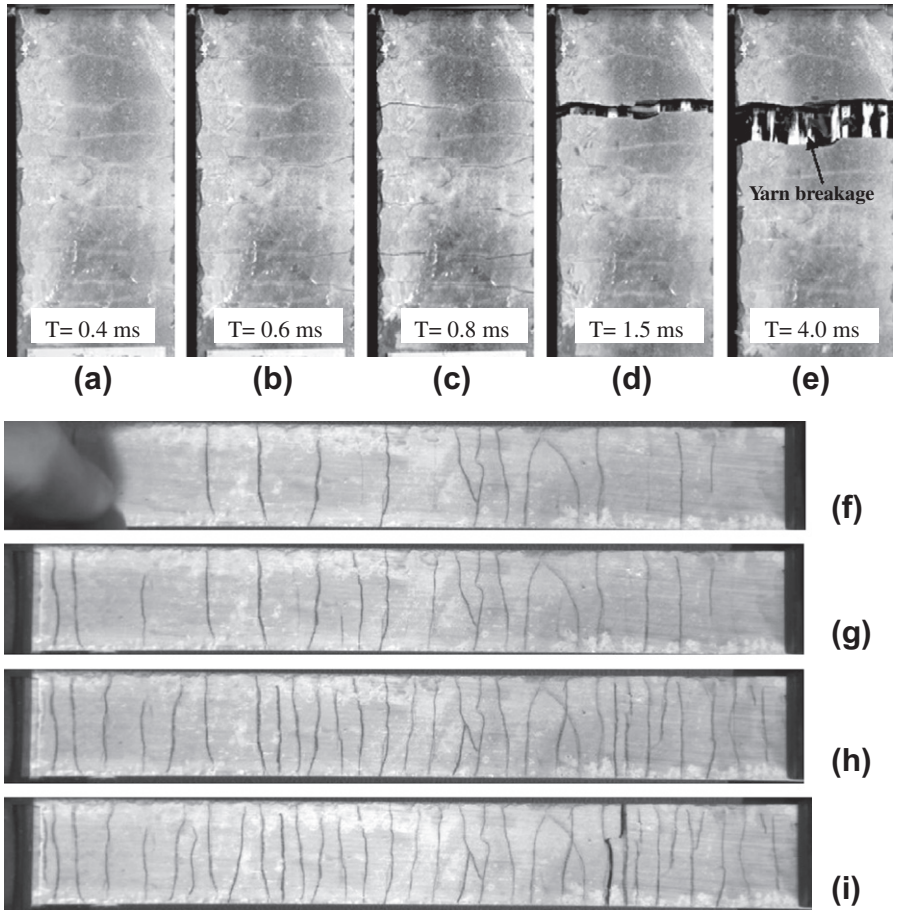


**Fig. 8.** Images of AR-glass composites under dynamic loading: (a–c) multiple micro-cracking, (d) main crack widening and other micro-cracks closing, (e) complete failure; and under static loading: (f–h) development of multiple micro-cracking, and (i) complete failure.

interference pattern on the surface of the object. Both laser beams go through a 50/50 beam splitter (C) which transmits one polarized beam, and reflects the other thus separating the two frequency components based on their orthogonal polarization. Mirrors (D) are used to make the transmitted and reflected beams parallel to one another. The beams reflected by the mirror intersect at one location on specimen surface where a moving fringe is formed. The beams reflected by 50/50 beam splitter also intersect on specimen surface and form a moving fringe. The lights scattered from both locations of specimen surface are detected by optical detectors (E) which generate independent signals characterizing the displacement at the point of measurement. A digital phase-meter in the control unit tracks the relative phase difference between the two detected signals and a reference signal. Surface displacement is measured for each of the two locations and the differential displacement (removing rigid body motions) is converted to an average strain between the points. The displacement measurement at each point is facilitated by interference of two beams of the laser light that meet at the sample surface at a fixed angle (Fig. 4). Interference fringe patterns are formed where the two beams overlap. The fringe spacing is given by

$$D_{fringe} = \lambda/(2\sin\phi) \tag{1}$$

where $\phi$ is the half angle between the two incoming beams and $\lambda$ is the laser wavelength [34].

In applications conducted under normal speed mode, the electronic control unit can convert the optical signals of laser extensometer into one analog or digital voltage output that is collected by a data acquisition device. However, due to the high strain rate, electronic processing of signals is not possible and a two-step process of high speed data acquisition followed by post-processing is necessary. Optical signals are converted by a high speed accessory and stored as electronic sinusoidal waves that are post-processed to obtain the displacements at both measurement points. This procedure is discussed in the following section.

### 3.2. Phase shift based on zero-crossing method

The detectors in the laser extensometer head measure two 250 kHz sinusoidal waves when the specimen is stationary. However as the specimen deforms under loading, the frequency of sinusoidal wave signals changes since it is a function of sample surface velocity [34]. The phase shift between the sinusoidal waves and the reference signal (250 kHz) was computed numerically using a zero-crossing method [35]. Fig. 5 illustrates the basic concept of phase shift based on zero-crossing method – a change in phase of a periodic signal with respect to a reference. By defining the parameters $x(i)$, and $x(i+1)$ as voltage signals at two subsequent time steps, the zero-crossing is defined by the following criteria:

$$\begin{aligned} &x(i)x(i+1) \leqslant 0 \quad \text{unbiased zero-crossing} \\ &x(i+1) - x(i) > 0 \quad \text{ascending} \\ &x(i+1) - x(i) < 0 \quad \text{descending} \end{aligned} \tag{2}$$

These zero-crossing locations are shown with an asterisk in Fig. 5. The phase shift between the reference signal and laser signal can be calculated as:

$$\theta_i = \frac{2\pi(T_{i+1} - T_i)}{T_{ref}} \tag{3}$$

where $\theta_i$ is the phase shift, $T_i$ and $T_{i+1}$ are the time when zero-crossing is detected by Eq. (2), and $T_{ref}$ is the period of reference signal (1/

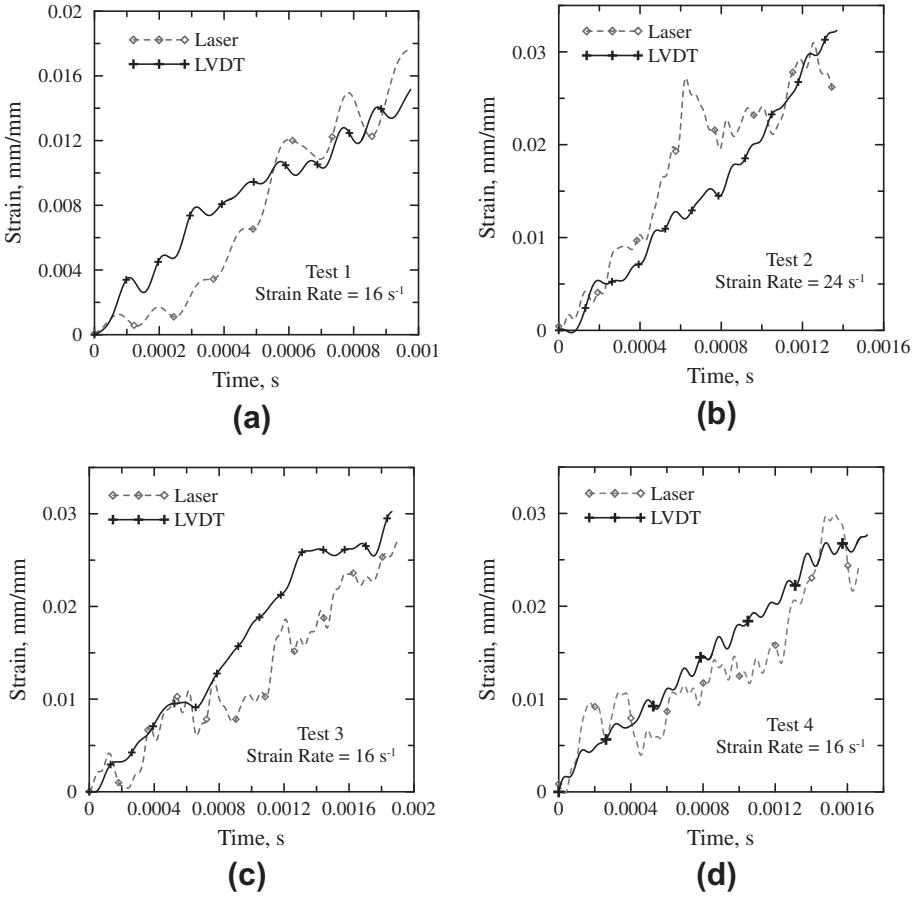


**Fig. 9.** Comparison of strain time histories of AR-glass fabric–cement composites measured by laser extensometer and Stroke LVDT.

250 ms). The phase shifts of both signals can be obtained with respect to the reference signal. The displacement of measurement point is directly proportional to the number of phase shift cycles and fringe spacing as:

$$D_i = \frac{\theta_i}{2\pi} D_{fringe} = \frac{(T_{i+1} - T_i)}{T_{ref}} D_{fringe} \quad (4)$$

where $D_i$ is the displacement of the measurement point on specimen surface, $\theta_i$ is the phase shift at current time step, and $D_{fringe}$ is the fringe spacing. When the relative phase increases by as much as one sinusoidal wave cycle, the measurement point moves a distance equal to the fringe spacing. The proposed phase shift technique has been successfully used in dynamic tensile testing of aluminum alloy 6061-T6 at strain rates from 25 to 210 $s^{-1}$ [36].

## 4. Experimental program of AR-glass fabric–cement composite

### 4.1. Test specimens

The AR-glass fabric–cement composites were prepared using a pultrusion process. The fabric passes through a slurry infiltration chamber to get coated and then is pulled through a set of rollers to squeeze the paste in between the fabric openings while removing excessive paste [37]. The fabric–cement composite is then formed on a plate shaped mandrel resulting in laminated sheets with 250 × 300 mm and thickness of about 10 mm. Cement sheets are made with four layers of fabrics. The reinforcing yarns of each fabric are placed along the pultrusion direction. After forming the samples, constant load of about 50 N is applied on the surface of the fabric–cement sheet to improve penetration of the matrix in between the yarn and fabric openings. All sheets are cured in water at room temperature for 28 days and then cut into 25 × 150 × 10 mm (width × length × thickness) pieces. Aluminum plates (25 × 50 × 1 mm) were glued onto the gripping edges of the composite specimen to minimize local damage and provide better load transfer in the grips (see Fig. 6a). The gage length of the composite specimen is 50 mm. A 42% cement, 5% silica fume, 0.1% superplasticizer and 50% water by volume mix design is used and the water/cement ratio by weight is 0.4. The laminated fabric–cement composite is a brittle matrix composite that exhibits matrix cracking and formation of a distributed array of micro-cracks with relative small failure strain [38].

The AR-glass fabric (Nippon Electric Glass Co., Ltd.) consists of orthogonal set of yarns (warp and weft) that are coated with sizing and bonded at the junction points. There are about 400 individual filaments each 13.5 μm in diameter in a fabric yarn resulting in a yarn diameter of 0.27 mm (see Fig. 6b). The yarns have a tensile strength of 1270–2450 MPa and modulus of elasticity of 78 GPa [37].

As shown in Fig. 7a, a specimen was held with low mass and high strength steel sockets and wedge frictional grips. Proper alignment of laser extensometer is achieved to obtain valid signals for strain measurement. Fig. 7b shows a small portion of the signals for post-processing, i.e. reference signal, signals 1 and 2 that are generated by the laser extensometer and the high speed accessory after receiving scattered light from the composite. The reference signal is artificially constructed and has a frequency of 250 kHz. Using the zero-crossing method (discussed in Section 3.2), the phase shift between signal 1 and the reference signal is calculated throughout the test duration. Similarly the phase shift between signal 2 and the reference signal is also calculated. The displacement is calculated using Eq. (4) for each location. The difference between two displacements represents the extension of the specimen and the engineering strain is calculated as

$$\varepsilon(t) = \frac{|D_1(t) - D_2(t)|}{L} \quad (5)$$

where $D_1(t)$ and $D_2(t)$ are the displacements of locations 1 and 2, respectively, and $L$ is the original distance between the two locations (25.4 mm).

**Table 1**
Maximum strain of the AR-glass fabric–cement composite measured by laser extensometer and Stroke LVDT.

| Strain rate ($s^{-1}$) | Maximum strain (mm/mm) | | |
|---|---|---|---|
| | Laser | Stroke LVDT | Difference |
| 16 | 0.0176 | 0.0152 | 0.0024 |
| 24 | 0.0258 | 0.0323 | −0.0065 |
| 16 | 0.0271 | 0.0302 | −0.0031 |
| 16 | 0.0246 | 0.0277 | −0.0031 |

### 4.2. Results and discussion

#### 4.2.1. Failure behavior

The failure behavior of the composite is recorded by a high speed digital camera (Phantom v.7) at a sampling rate of 10,000 fps. Typical images were chosen to present the cracking pattern of the composite as shown in Fig. 8. Note that there are three stages in the failure of the composite during the loading pro-

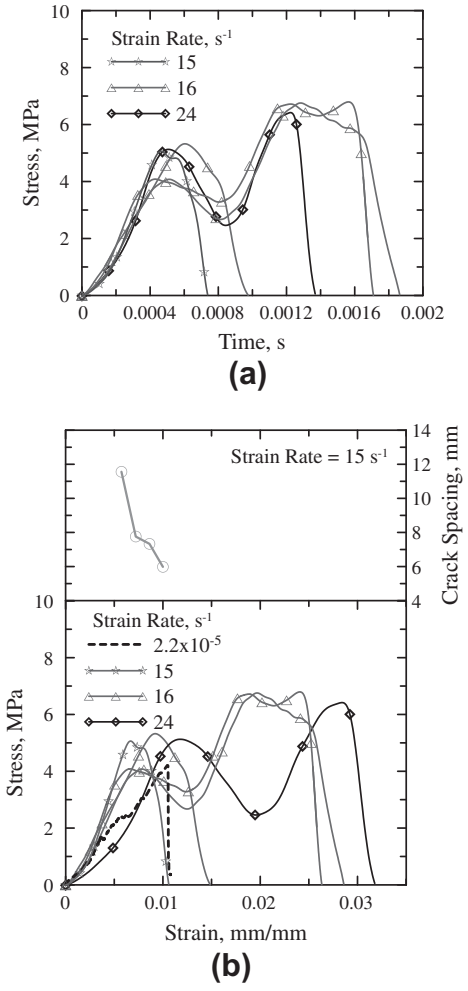


**Fig. 10.** Response of AR-glass fabric–cement composite at different strain rates: (a) stress–time, and (b) stress–strain and crack spacing.

**Table 2**
Dynamic and static material properties of AR-glass fabric–cement composite.

| Loading condition | Test no. | Strain rate ($s^{-1}$) | Young's modulus (MPa) | Tensile strength (MPa) | Toughness (MPa) | Max. strain (mm/mm) |
|---|---|---|---|---|---|---|
| Dynamic | 1 | 16 | 639 | 5.32 | 0.044 | 0.0152 |
| | 2 | 24 | 660 | 6.42 | 0.109 | 0.0323 |
| | 3 | 16 | 767 | 6.76 | 0.110 | 0.0302 |
| | 4 | 16 | 831 | 7.42 | 0.111 | 0.0277 |
| | 5 | 15 | 1054 | 5.06 | 0.028 | 0.0106 |
| | Avg. | 17 | 790 | 6.20 | 0.080 | 0.0232 |
| | Std. dev. | 4 | 167 | 0.99 | 0.041 | 0.0098 |
| Static | Avg. | $2.2 \times 10^{-5}$ | 376 | 4.11 | 0.024 | 0.0103 |
| | Std. dev. | – | 16.5 | 0.25 | 0.002 | 0.0007 |

cess. Fig. 8a–c represents the developing of the multiple cracking process. The behavior of successive cracking is indicative of stress transfer mechanism at the fabric–cement interface to be sufficient for load transfer and composite action. After this stage, the strain increases and cracks open uniformly until the bifurcation point. At this stage one of the cracks becomes the dominant one that continues to open while the load begins to decrease. This dominant crack is clearly visible while all other cracks appear to close Fig. 8d–e. The main crack continues to widen under load for the duration of the test. At this point the forces are mainly carried by the fabric until all its yarns are completely broken (Fig. 8e) leading to a complete failure of the composite. Similar behavior is also observed under static loading such as progressive multi-cracking developments (Fig. 8f–h) and one dominant crack leading to final failure (Fig. 8i).

*4.2.2. Stress–strain response and cracking*

Fig. 9a–d shows the comparison of strain time histories of four test cases for AR-glass fabric–cement composite measured by the Stroke LVDT and the laser extensometer at an average strain rate of 17 $s^{-1}$. It should be noted that the strain time history curves of composite specimens have a wavy pattern due to axial oscillations of the test frame. Each strain time history curve corresponds well with strain values measured by both methods. Table 1 summaries the maximum strain values of the composite obtained by both measurements at various strain rates. If the surface of composite specimen has large defects, the quality of signals can be influenced significantly causing inaccurate strain measurements.

The stress–time and stress–strain curves of several specimens at three strain rates: 15, 16 and 24 $s^{-1}$ are shown in Fig. 10a and b. The response of individual specimens is quite different. The test durations of two tests are less than 0.1 ms and there is only one peak in the stress indicating that all four layers of AR-glass fabric in the composite broke simultaneously. However, for the remaining three specimens there are multiple peaks in the stress–strain curves, indicating sequential failure of fabric layers. The dynamic material properties of the fabric–cement composite are summarized in Table 2. The Young's modulus is 790 ± 161 MPa, tensile strength is 6.20 ± 0.99 MPa, and the toughness (the area under stress–strain curve) is 0.08 ± 0.041 MPa.

The typical stress–strain response of the composite under quasi-static loading is also plotted in Fig. 10b. The composite under dynamic loading is 21% stronger, the maximum strain is approximately twice as large and the toughness is almost three times as large compared to the performance under quasi-static loading. The accuracy required in quantifying relative improvements in mechanical properties necessitates the various methods of measuring the displacement and strain rate properties. The averaged static properties of the composites were also included in Table 2. There are several possible reasons for the strain rate dependency of the composites. First, the AR-glass fabric itself used in the composite is rate sensitive due to the nature of polymeric phase of sizing which bonds the warp and fill yarns [39]. Experimental data shows that the Young's modulus of the fabric increased from 97.4 ± 8.9 GPa to 118.5 ± 10.3 GPa, tensile strength from 2.76 ± 0.37 GPa to 3.27 ± 0.22 GPa, maximum strain from 0.036 ± 0.002 mm/mm to 0.05 ± 0.002 mm/mm, and toughness from 52.8 ± 8.6 MPa to 90.0 ± 9.0 MPa, when the strain rate increases from $8.0 \times 10^{-5}$ $s^{-1}$ to 20 $s^{-1}$. Second, the debonding at the interfaces between the fabric and cement matrix may contribute to rate sensitivity. Mechtcherine et al. [23] found a significant increase (by approximately a factor of 2) of the maximum force before interfacial debonding occurs when the strain rate is increased for PVA fiber embedded in cement matrix. An increase in the loading rate appears to enhance interface bonding strength due to the creep effects in load transfer mechanism at fiber–matrix interface. An improved understanding of this phenomenon can take place by conducting fabric pullout test from cement paste matrix at different loading rates.

The calculated crack spacing based on captured images at a strain rate of 15 $s^{-1}$ (test 5) is correlated with the applied strains and plotted together with the stress–strain responses in Fig. 10b. Average crack spacing decreases from 11.6 mm to 6 mm when the strain increases from 0.006 to 0.01 indicating the progressive development of cracks during the loading process.

## 5. Conclusions

Non-contact measurements (laser extensometer and DIC method), although labor intensive, present alternatives to the Stroke LVDT measurement using the actuator displacement [25]. Whereas the laser extensometer has no apparent advantages over the Stroke LVDT measurement, it serves as an accurate means for checking such stroke measurements for high rates of loading. The DIC method gives full-field displacement and strain values to better understand the local failure of cement-based composites under both quasi-static and dynamic tensile testing. Several points can be noted from the present work.

(1) Non-contacting strain measurement procedure using phase-shift technique is an independent method that can be used in dynamic tensile testing of cement-based composites. The image analysis on sisal fiber cement composite shows that the Stroke LVDT measurement in the high strain rate testing system is sufficiently accurate to evaluate the dynamics response.
(2) The strain time histories of AR-glass fabric–cement composite specimens at an average strain rate of 17 $s^{-1}$ measured by the laser extensometer match those measured by the Stroke LVDT, demonstrating the workability of the proposed procedure in dynamic tensile testing.
(3) The mechanical properties of AR-glass fabric–cement composite are sensitive to strain rate. The Young's modulus, tensile strength, maximum strain, and toughness under

dynamic loading are higher than those under quasi-static loading. The accuracy required in quantifying relative improvements in mechanical properties necessitates the various methods of measuring the displacement and strain rate properties.

(4) The strain hardening composites exhibit a stiff response initially followed by distributed microcracking and formation of a single dominant crack that leads to final failure under both static and dynamic loadings, illustrated by images captured during tests. The progressive development of cracks during loading process indicates sufficient stress transfer at the fabric–cement interface.

(5) Both the laser extensometer and image analysis are effective as alternate displacement measurements for high strain rate testing. These measurements validate the results obtained by the Stroke LVDT. The accuracy of laser extensometer depends on the quality of acquired signals. The acquired data can be filtered and fitted to construct the stress–strain curve. DIC-based image analysis procedure may be preferable to Stroke LVDT and laser measurements as it is a full-field measurement and provides information of local failure. The machine compliance does not affect the accuracy of strain/displacement measurement for cement-based composite at the investigated strain rates as both the Stroke LVDT and laser measurements provide consistent results.

## Acknowledgments

The authors wish to thank William Emmerling, Donald Altobelli and Chip Queitzsch of the Federal Aviation Administration's Aircraft Catastrophic Failure Prevention Research Program for their support and guidance. Partial funding for this effort was provided by the FAA. The authors would like to thank Dr. Alva Peled for providing the AR-glass fabric–cement composites.

## References

[1] Nicholas T. Tensile testing of material at high rates of strain. Exp Mech 1981;21(5):177–85.
[2] Benloulo ISC, Rodriguez J, Martinez MA, Galvez VS. Dynamic tensile testing of aramid and polyethylene fiber composites. Int J Impact Eng 1997;19(2):135–46.
[3] Zhu D, Gencoglu M, Mobasher B. Low velocity impact behavior of AR-glass fabric reinforced cement composites in flexure. Cem Concr Compos 2009;31(6):379–87.
[4] Kenneth GH. Influence of strain rate on mechanical properties of 6061–T6 aluminum under uniaxial and biaxial states of stress. Exp Mech 1966;6(4):204–11.
[5] Zabotkin K, O'Toole B, Trabia M. Identification of the dynamic properties of materials under moderate strain rates. In: 16th ASCE engineering mechanics conference. Seattle, WA; 2003.
[6] Extensometers and Clip Gage Catalog. MTS system corporation, Minneapolis, MN; 1993.
[7] Strain gage technology. Measurements group. Raleigh, NC; 1993.
[8] Bastias PC, Kulkarni SM, Kim KY, Gargas J. Non-contacting strain measurements during tensile tests. Exp Mech 1996;36(1):78–83.
[9] Anwander M, Zagar BG, Weiss B, Weiss H. Non-contacting strain measurements at high temperatures by the digital laser speckle technique. Exp Mech 2000;40(1):98–105.
[10] Verleysen P, Degrieck J. Optical measurement of the specimen deformation at high strain rate. Exp Mech 2004;44(3):247–52.
[11] James FB. On the direct measurement of very large strain at high strain rate. Exp Mech 1967;7(1):8–14.
[12] Choi D, Thorpe JL, Hanna RB. Image analysis to measure strain in wood and paper. Wood Sci Technol 1991;25(4):251–62.
[13] Aydilek HA, Guler M, Edil TB. Use of image analysis in determination of strain distribution during geosynthetic tensile testing. J Comput Civil Eng 2004;18(1):65–74.
[14] Maalej M, Quek ST, Zhang J. Behavior of hybrid-fiber engineered cementitious composites subjected to dynamic tensile loading and projectile impact. J Mater Civil Eng 2005;17(2):143–52.
[15] Mechtcherine V, Millon O, Butler M, Thoma K. Mechanical behaviour of strain hardening cement-based composites under impact loading. Cem Concr Compos 2011;33(1):1–11.
[16] Mobasher B, Peled A, Pahilajani J. Distributed cracking and stiffness degradation in fabric–cement composites. Mater Struct 2006;39(3):317–31.
[17] Peled A, Bentur A. Fabric structure and its reinforcing efficiency in textile reinforced cement composites. Composites Part A 2003;34:107–18.
[18] Candoni E, Labibes K, Albertini C, Berra M, Giangrasso M. Strain-rate effect on the tensile behaviour of concrete at different relative humidity levels. Mater Struct 2001;34(1):21–6.
[19] Xiao S, Li H, Lin G. Dynamic behaviour and constitutive model of concrete at different strain rates. Mag Concr Res 2008;60(4):271–8.
[20] Kim DJ, El-Tawil S, Naaman AE. Rate-dependent tensile behavior of high performance fiber reinforced cementitious composites. Mater Struct 2009;42(3):399–414.
[21] Silva FA, Zhu D, Mobasher B, Soranakom C, Toledo Filho RD. High speed tensile behavior of sisal fiber cement composites. Mater Sci Eng: A 2010;3(15):544–52.
[22] Zhu D, Peled A, Mobasher B. Dynamic tensile testing of fabric–cement composites. Constr Build Mater 2011;25(1):385–95.
[23] Mechtcherine V, Silva FA, Butler M, Zhu D, Mobasher B, Gao S, et al. Behaviour of strain-hardening cement-based composites under high strain rates. J Adv Concr Technol 2011;9(1):51–61.
[24] Silva FA, Butler M, Mechtcherine V, Zhu D, Mobasher B. Strain rate effect on the tensile behaviour of textile-reinforced concrete under static and dynamic loading. Mater Sci Eng: A 2011;528(3):1727–34.
[25] Borsutzki M, Cornette D, Kuriyama Y, Uenishi A, Yan B, Opbroek E. Recommendations for dynamic tensile testing of sheet steels. International Iron and steel institute; 2005.
[26] Zhu D, Rajan SD, Mobasher B, Peled A, Mignolet M. Modal analysis of a servo-hydraulic high speed testing machine and its application to dynamic tensile testing at an intermediate strain rate. Exp Mech 2011;51(8):1347–63.
[27] Madisetti VK, Williams DB. The digital signal processing handbook. CRC Press; 1998.
[28] Zhu D, Mobasher B, Rajan SD. Dynamic tensile testing of Kevlar 49 fabrics. J Mater Civil Eng 2011;23(3):230–9.
[29] Kobayashi AS. Handbook on experimental mechanics. 2nd ed. New York: Society for experimental mechanics; 1993.
[30] Peters WH, Ranson WF. Digital imaging techniques on experimental stress analysis. Opt Eng 1982;21(3):427–31.
[31] Sutton MA, Wolters WJ, Peters WH, Ranson WF, McNeill SR. Determination of displacement using an improved digital correlation method. Image Vision Comput 1983;1(3):133–9.
[32] Poissant J, Barthelat F. A novel subset splitting procedure for digital image correlation on discontinuous displacement fields. Exp Mech 2010;50(3):353–64.
[33] Mobasher B, Rajan SD. Image processing applications for the study of displacements and cracking in composite materials. In: 16th ASCE engineering mechanics conference (EM 2003). Seattle, WA; 2003.
[34] Laser Extensometer 3000 Operation & Maintenance Manual. OPTRA, Inc.
[35] Vainio O, Ovaska SJ. Noise reduction in zero crossing detection by predictive digital filtering. IEEE Trans Indus Electron 1995;42(1):58–62.
[36] Zhu D, Mobasher B, Rajan SD, Peralta P. Characterization of dynamic tensile testing using aluminum alloy 6061-T6 at intermediate strain rates. ASCE J Eng Mech, in press. doi:10.1061/(ASCE)EM.1943-7889.0000264.
[37] Peled A, Mobasher B. Pultruded fabric–cement composites. ACI Mater J 2005;102(1):15–23.
[38] Peled A, Mobasher B. Tensile behavior of fabric cement-based composites: pultruded and cast. ASCE J Mater Civil Eng 2007;19(4):340–8.
[39] Soranakom C, Mobasher B. Modeling of tension stiffening in reinforced cement composites: Part I – theoretical modeling. Mater Struct 2010;43:1217–30.